Postprint of: Jendrzejewski R., Kreja I., Śliwiński G., Temperature distribution in laser-clad multi-layers, Materials Science and Engineering: A, Vol 379, iss. 1–2 (2004), pp. 313-320, DOI: 10.1016/j.msea.2004.02.053

Temperature distribution in laser-clad multilayers

R. Jendrzejewski [a,*], I. Kreja [b] and G. Śliwiński [a]

[a] Polish Academy of Sciences, Institute of Fluid-Flow Machinery,
Fiszera 14, PL 80-231 Gdańsk

[b] Gdańsk University of Technology, Faculty of Civil Engineering,
Narutowicza 11/12, PL 80-952 Gdańsk

ABSTRACT

Results of temperature distribution modelling for multilayer structures prepared by direct laser remelting of metal powders in an Ar environment were numerically obtained and compared with experimental data. Powders of bronze B10 and stellite SF6 alloys and also base plates of S235JR steel were taken as sample materials. In the experiment a 1.5 kW cw CO_2 laser, equipped with a multi-stream nozzle capable of delivering metal powder at a rate of up to 0.2 g/s coaxially with the laser beam, was used. Dimensions of the melted zone and its position relative to the base were obtained from calculation and agree with the microstructure observation of the sample cross-sections. The model revealed that isotherms at 1020 °C and 1350 °C penetrate the interfaces to a depth of about 5-10% of the individual layer height for B10 and SF6, respectively. This was confirmed by inspection in a scanning electron microscope (SEM) and also by a depth-dependent X-ray Energy-Dispersive Spectroscopy (XEDS) measurement of the main chemical components of multilayers, i.e. Fe, Co, Ni (SF6) and Fe, Cu, Sn (B10). Also the cooling rates indicated agreement between modelling and experiment. This allows us to conclude that the model can be applied for pre-selection of the process parameters.

Keywords: laser cladding, temperature field modelling, multilayers

* Corresponding author: phone: +48 58 3411271, fax: +48 58 3416144, e-mail: rafj@imp.gda.pl

1. INTRODUCTION

There is a growing interest observed in application of laser cladding of metal powders for production of protective coatings, e.g. on steam turbine blades and valve seats as well as in the repair of damaged machine parts [1-3]. A particular interest is devoted to coatings made of materials showing good performance under extreme operating conditions, such as high temperature erosion, aggressive environment, exposure to intense wear attack, etc. The results published so far are limited to selected materials. For example, stellite coatings which exhibit a relatively high wear resistance comparable with that of TiN alloys seem to be well suited for the mentioned applications [2].

It has been shown for some materials that the technique can also serve as an efficient tool for rapid manufacturing of models, prototypes and functional 3-D elements [3-5]. Intensive investigations are stimulated by the needs for cost-effective production techniques, which become an important market sector nowadays.

However, correct selection of process parameters for preparation of spatial structures of required geometry is quite a difficult task. Quantities such as the laser beam power, beam intensities in the processing zone, scanning speed and powder feed-rate depend on each other via mutual interaction and influence strongly the remelted material properties. For example, an insufficient intensity of the laser beam may result in a lack of melting and insufficient bond of consecutive layers. On the other hand, a deeper penetration and remelting due to higher beam intensities lead to lowering of the structure quality.

A literature review has shown that descriptions and theoretical models considered concern usually the laser cladding of a single layer of metal powder. In addition, the majority of published solutions are limited to a simplified case of fixed geometry for an autonomic, lateral nozzle [6-8].

In the multi-layer case one should include the phenomenon of laser remelting of subsequent layers, which makes the model considerably more complex. For subsequent layers the growing distance from the base hinders heat conduction and promotes the convection and radiation mechanisms [9]. An analysis of a single layer problem can be performed for the reference frame fixed to the laser beam and the problem can be reduced to solving a stationary process. In contrary, for a model of multilayer production by subsequent melting of individual layers it is necessary to know the temperature at a specific point of the applied layer. This temperature is a function of time elapsed since production of the fragment below which belongs to the underlying, previously produced layer. For the above reasons a model with the reference frame fixed to the produced structure can be considered a better choice.

In this paper modelling of the temperature distribution in laser-cladded multilayer structures is presented and discussed. Results obtained numerically for sample materials such as bronze B10 and stellite SF6 are compared with experiment. From the model the shape and dimensions of the molten pool, together with the inter-layer dilution coefficient are determined based on the location of isotherms. The respective experimental results are extracted from the SEM observations of sample cross-sections and XEDS (X-ray Energy-Dispersive Spectroscopy) analysis of the chemical composition of the clads. Moreover, the cooling curves evaluated by numerical calculations and also cooling rates are compared with the measured data.

2. TEMPERATURE FIELD MODELLING

For the processing region it is assumed that an annular nozzle coaxial with the laser beam delivers the powder vertically down to the workpiece which is mounted on an xy-table and can be moved at a controlled speed. In the vicinity of the deposition plane the powder jet traverses partially the laser beam prior to impinging on the surface. The powder part reaching

the melt pool is obtained from geometrical considerations and in the modelling this material only contributes to the melt volume. It is postulated that the processing speed is sufficiently low to assume that the thermal diffusion prevails in the heat transfer, and the powder particles remain in the pool sufficiently long to be liquefied. This means that prior to melting of the actually supplied powder particles the pool contains a two-phase material, which is instantaneously mixed and becomes liquid due to the laser action. This implies also that parameters related to the powder jet, such as the particle spatial distribution and density can be neglected. For the laser beam a triangular profile corresponding to an approximation of the Gaussian intensity distribution is assumed.

Under these assumptions a simplified problem description may be adopted. The problem can be described by the energy conservation and mass balance equations

$$\frac{\partial \mathrm{T}}{\partial \mathrm{t}} = \nabla\left(\kappa \nabla \mathrm{T}\right) + \frac{\mathrm{Q}}{\rho \mathrm{C}} - \left(v_{\mathrm{SC}} \nabla\right)\mathrm{T}, \tag{1}$$

$$\frac{\partial \rho}{\partial \mathrm{t}} + \nabla\left(\rho v_{\mathrm{SC}}\right) = 0, \tag{2}$$

where Q is the heat generated per unit volume, v_{sc} stands for the surface scanning velocity, and C, ρ and κ are the material dependent coefficients: specific heat, density, and heat conductivity, respectively.

By introducing the thermal conductivity of the material, $\lambda=\kappa\rho C$, and taking into account that the laser beam represents the only heat source, i.e. the term $\left(v_{\mathrm{SC}} \nabla\right)\mathrm{T}$ equals 0, equation (1) can be rewritten in the form

$$\rho \mathrm{C} \frac{\partial \mathrm{T}}{\partial \mathrm{t}} = \nabla\left(\lambda \nabla \mathrm{T}\right) + \mathrm{Q}. \tag{3}$$

A similar approach was extensively discussed in [8] for the case of a single layer laser cladding.

The interaction region under consideration and the laser beam position relative to the multilayer are shown schematically in Fig. 1. Numbers in circles denote the base (⓪) and consecutive layers (①-③).

Equation (3) should be supplemented with an appropriate boundary condition for the component of the laser power flux in a direction normal to the upper surface of the molten pool

$$-\lambda \frac{\partial T}{\partial n} = q_l - \chi\left(T_S - T_0\right), \tag{4}$$

$$\lambda_s \frac{\partial T_s}{\partial n} - \lambda_l \frac{\partial T_l}{\partial n} = V_m \rho L \qquad \text{for } T=T_m, \tag{5}$$

where q_l is the laser intensity absorbed by the irradiated surface or interface, χ represents the surface-related heat transfer coefficient, $\partial T/\partial n$ are the temperature gradients normal to the solid-liquid interface, T_0, T_S, T_m are the ambient, irradiated surface and melting point temperature values, respectively. V_m stands for velocity of the phase change interface, L for the latent heat, and subscripts s and l refer to the solid and liquid phase, respectively.

The numerical model of the heat transfer [5, 10] adopted in the paper accounts for the phase change phenomenon in the fixed mesh approach. Temperature dependent material properties as well as convective and radiative boundary conditions are included.

3. RESULTS OF MODEL CALCULATIONS

Numerical evaluation of the temperature distribution has been carried out with the computer code NHTVSAP (Non-linear Heat Transfer Variable Step Analysis Procedure) [10]. It enabled analysis of the 2-D heat transfer problem for a fixed domain, taking into consideration the phase change and the heat exchange with the environment for a given, local set of boundary conditions. The procedure bases on an approach discussed e.g. in [11].

In solving equation (3) the non-linear, temperature-dependent material properties were taken into account. The boundary conditions were introduced into the model equations through parameter values, and calculations were performed by means of the Euler-backward, implicit time-integration. Due to the non-linearity of the problem and because of the time dependence of the parameters it was necessary to combine the numerical integration with Newton-Raphson equilibrium iterations.

The treatment of the phase change assumes that the temperature gradient is normal to the phase change interface. A fixed mesh of 8-node isoparametric finite elements used for the discretization of the temperature field analyzed is combined with 3-node interface element modelling of the movement of the phase change front. According to the type of intersection, the "mother" element is divided into quadrilateral and/or triangular sub-elements. A special procedure is used to build solution matrices for discontinuous elements intersected by the moving phase change boundary.

The calculation area for consecutive steps was defined through setting of individual node co-ordinates and spanning the 8-node quadrilateral element mesh over them. Every subsequent layer of the melted material had its equivalent in at least one mesh row. For each individual layer a new, modified mesh was used, while the sum of the mesh row heights related to the base was kept constant. The thickness of the cladded layer h_c was calculated from the mass conservation equation (2) in the form

$$h_c = \frac{\eta m_p}{b \rho_c v_{sc}}, \tag{6}$$

where η denotes the powder efficiency, i.e. the ratio of the powder adhered to the workpiece to that supplied in the jet, ρ_c stands for the powder material density, m_p is the powder feed-rate, and b represents the trace width. The powder efficiency η was obtained in dependence on the geometry of the powder jet and laser beam interaction region. It was approximately equal to the ratio of the cross-section areas of laser beam and the powder jet at

a given distance from the nozzle outlet. For different powder materials and values of m_p, the corresponding area ratio varied between 0.23 and 0.26 [5].

The scanning speed was specified by the time and space intervals between consecutive nodes. The initial and environmental temperatures, and also the laser beam power were taken from the experiment. The material constants were adopted from data bases or estimated on the basis of mild steel properties and are collected in Table 1. For the temperature dependent thermal conductivity λ and heat capacity C the ranges of values applied in calculation were given. In different meshes of the created net these parameters corresponded to the base (denoted by ⓪) or cladd materials (layers ①-④).

The χ coefficient was taken equal to 100 $W/m^2 \cdot deg$ [8] for all materials. The absorbed laser intensity q_l was calculated as product of the absorption coefficient A and the laser beam intensity I. For A values of 18-19% were taken from literature [5, 6], and the laser intensity I was calculated from experiment using the relationship $I=4P/\pi b^2$.

The initial temperature for a given location of the consecutive layers was taken equal to the value obtained from the time dependent cooling curve, i.e. according to the time elapsed since the preparation of the corresponding location of the underlying, previously remelted layer. In the case of bronze B10 the calculations were performed for m_p=0.2 g/s, v_{sc}=16.7 mm/s, and P=605 W, for which the layers of thickness h_c equal to 0.6 mm were experimentally obtained. For stellite the values of m_p=0.16 g/s, v_{sc}=11.7 mm/s, and P=800 W, corresponding to h_c=0.4 mm [5] were used. The operation range of the parameters was estimated from experiment.

In the diagrams showing the results of model calculation (Figures 2-5) the dimension lines relate to the finite element mesh and also indicate the layer and base thickness equal to 0.6 mm and 1.8 mm for bronze B10, and 0.4 mm, 1.8 mm for stellite SF6 layers and steel base, respectively. The vertical, dashed line above the mesh represents the current position of

the laser beam axis. Temperatures are given in Celsius degrees. Temperature fields during cladding of the first bronze B10 layer after 180 and 270 ms are shown in Fig. 2a and in Fig. 2b, respectively. In both cases the position of the 1500 °C isotherm, corresponding to the melting temperature of the base material, delivers information on the melt pool dimension. This is of importance when remelting of the neighbouring layers should be considered due to the material properties required after multilayer preparation. The isotherm penetrates the base to a depth of about 5-10 % of the layer height. This corresponds to the partial melting of the base and assures a good bond of the first layer; it also confirms the correctness of the assumed model parameters. In the highest temperature zone the temporal temperature changes are moderate. However, after a prolonged processing time of 270 ms the positions of the isotherms at 800, 600, and 400°C indicate substantial base heating – see Fig. 2b.

Temperature distributions calculated for the second and fourth bronze layers at a time of 0.27 s (from the start of calculations) are shown in Fig. 3. These results can be additionally compared with those shown for the first layer in Fig. 2b. For modelling of the consecutive bronze B10 layers, the applied laser beam power is reduced by 30% compared to that adopted for the first layer and the value of q_l is changed accordingly. This reduction prevents overheating of the existing layer and corresponds to the experimental conditions. It can be concluded from Fig. 3, based on the position of the 1000 °C isotherm and noting that the bronze melting point corresponds to 1020 °C, that a partial melting of the previous layer occurs. The differences in the isotherm location observed for subsequent layers result from the surface preheating due to the production of the first layer, and from reduction of the heat conduction to the base with a growing thickness of the multilayer – compare Figures 2b and 3a,b.

The temperature distributions for the second layer of laser-cladded stellite SF6 at two selected time instants of 0.22 s and 0.35 s are presented in Fig. 4. Results obtained after 0.35 s

of the processing time can be compared with those calculated for the first and fourth stellite layers – see Figures 4b and 5. In the case of stellite for the second and next layers, the laser beam power is reduced by 20% compared to that applied for the first layer. In Fig. 5a the 1500 °C isotherm corresponding to the base melting temperature reaches the base, and in other diagrams in Figures 4, 5 the 1350 °C isotherm, corresponding to the stellite melting point, penetrates the area of the underlying, previously remelted layer. In both cases the model confirms existence of a remelted interface between the substrate and the first layer, as well as between individual layers. The dilution coefficient value of about 5-10 % can be estimated for SF6, similarly to the B10 case. The result obtained for consecutive layers 2-4 indicates in agreement with the model assumption, that in this case the laser power should be suitably lower than that taken for calculation of the first layer – see Fig. 5b. This assures similar melting conditions and dilution coefficient during cladding of the consecutive layers, and is in part due to the higher melting point of the base compared with that of the cladded material. The resulting heating of the first layers (Figures 2, 5a) is more intense than heating of subsequent layers (Figures 3, 4, 5b), which follows from deeper penetration of appropriate isotherms in the first case.

4. EXPERIMENTAL

The laser-cladded structures were produced by using sample materials and processing conditions corresponding to the input data of calculated examples. Powders of bronze B10 (“Trzebinia” Metallurgical Works) and stellite SF6 (Deloro Stellite Ltd) were selected for the experiment. Properties and chemical composition of the original material applied are given in Table 2.

The experiment was carried out using a stand described in detail elsewhere [5, 12] and only a brief description of the set-up is given here. A workstation with a 1.5 kW continuous

wave (cw) CO_2 laser, equipped with a CNC-controlled manipulation table, was used for sample coating preparation. The laser head with a conical, water-cooled, multi-stream nozzle and a gravitational powder supply served for powder feeding coaxially with the laser beam axis. The configuration assured a well localized powder stream perpendicular to the processed surface and the technological result was independent of the workpiece direction of motion. Technically pure argon was used for metal powder transport as well as for shielding of the focussing lens and interaction zone. Values of the powder feed rate m_p ranged from 0.05 to 0.2 g/s. The laser beam power was controlled in the range of 0.4÷1.1 kW with an accuracy of ± 2%. The width b and thickness h_c of a single, remelted track were equal to 1 mm and 0.2 - 0.6 mm, respectively. The multilayer structures of a required thickness were produced by repeating the track structure after a stepwise, vertical movement of the sample under preparation. This assured controllable conditions in the powder jet – laser beam interaction zone for consecutive layers. In this way each subsequent layer was produced on the upper surface of the underlying, previous one until the required total height was reached. Values of the horizontal scanning speed v_{SC} were selected between 10 and 20 mm/s depending on the material, powder feeding rate and laser beam parameters.

The process conditions such as the laser beam power and the beam intensities in the processing zone, as well as the horizontal feed rate (scanning speed) for given values of m_p and b, were chosen experimentally in order to obtain correct remelting, a regular structure and track inter-connection via fusion zones. Following the conclusions from the model calculations the laser beam power applied to production of the second (upper) and next layers of stellite SF6 and bronze B10 was reduced to 80%, and 70%, respectively, of the value used for the first (lower) layer. These values were selected according to differences in melting points between the base material and stellite (150 °C) and between the base material and bronze (480°C). Plates of S235JR steel (bal. Fe, max. 1.1% Mn, max. 0,35% Si,

max. 0.3% Cr, max. 0.3% Cu, max. 0.3% Ni, max. 0.22% C) 1.8 mm thick were used as the base material.

The rates of temperature decrease after preparation of individual layers, i.e. the cooling rates, were measured with a Kleiber 270B fast pyrometer equipped with infrared macro-optics and characterized by the response time of 15 μs. The pyrometer signal was collected from a 0.8 mm spot at a fixed surface point of the layer just produced. Before measurement the pyrometer was calibrated by means of the Fe-CuNi thermocouple and the emissivity was adjusted in dependence on the material investigated.

After preparation of the samples for metallographic analysis their surface, cross-sections and fractures were investigated using optical, SEM and XEDS techniques.

5. RESULTS AND DISCUSSION

In order to check the correctness of the time-dependent temperature-field model the quantities characterizing the cladding process measured in the experiment and also the coating properties were analyzed and compared with data obtained from the calculations.

The most important experimental data regarding the multilayer and melt pool geometry were obtained from optical studies of sample microstructures. Dimensions of interest were extracted from microphotographs of the sample cross-sections, where the height of individual layers and the interlayer fusion zones are well resolved. A fragment of the fracture of a stellite multilayer composed of several, consecutively melted single-layers representing the uppermost three layers and the corresponding, magnified cross-section are shown together with a scheme of the structure in Fig. 6. The darker, horizontal regions in Fig. 6b correspond to the remelted material, i.e. fusion zones. Their heights amount each to (7±2)% of the height of an individual layer.

This observation coincides with the calculated location of the 1350°C isotherm penetrating the base-coating interface, for layers 1, 2 and 3, 4, which is shown as a time dependent temperature field in Figures 5a, 4 and 5b, respectively. This temperature value corresponds to the stellite melting point and the calculated temperature distribution is confirmed by the metallurgical bonds between individual layers via fusion zones observed in the experiment. From the model calculation the dilution coefficient taken as the largest depth of isotherm penetration into the underlying material can be estimated as h_b/h_c = (5-10)%. Also for multilayer coatings made of bronze B10, which is characterized by the melting point at 1020°C, similar values of this ratio are derived – see Figures 2 and 3. These results indicate agreement of estimations obtained both from the experiment and modelling.

Another experimental result for the h_b/h_c ratio follows from the XEDS analysis for the proximity of the layer-base interface. The dimension of interest is obtained from the depth-dependent sampling of the migration range of elements due to thermal processes in the melting pool. Results of elemental analysis, given as the percentage content of Fe, Co, Ni and Fe, Cu, Sn vs. distance from the interface, are shown in Fig. 7a and b for SF6 and B10 layers, respectively. From the diagrams the values of about 35 μm (SF6) and 16 μm (B10) for the vertical dimension of the dilution zone depth may be derived. This corresponds to the h_c/h_b ratio below 9%. The value obtained from XEDS agrees within the experimental error with that obtained from microphotographs and confirms again the correctness of the modelling.

Results of numerical calculations performed for both sample materials make also possible determining the cooling curves for consecutive layers. Appropriate data are obtained for a given set of points of crossing the upper surfaces of individual layers of the multilayer structure by a line normal to them.

The cooling rates of interest for structures composed of 4 layers can be derived from Fig. 8a, and b, for the bronze and stellite, respectively. The surface temperatures at the very

beginning of the process, i.e. corresponding to the lowermost layers of both materials are higher than those of higher lying layers. This is consistent with the assumed process conditions for the model, following from the experiment [5]. Small temperature differences observed for consecutive layers in Fig. 8 are caused by different initial temperatures during cladding of consecutive layers as well as by differences in conditions of heat conduction to the base. The calculated data shown on the graphs can be easily fitted; tangents to the fits of the cooling curves represent values of the cooling rates at given time instants. Values calculated for the first bronze layer change with time from 4200 °C/s to 1500 °C/s. For consecutive layers a change from 3400 to 1250 °C/s, similar in character, is derived from Fig. 8a. Correspondingly, the cooling rate for the first stellite layer varies from 4500 to 1450 °C/s, and from 3600 to 1350 °C/s for the next layers. These values obtained from model calculations are consistent with literature data on the cooling rates, which additionally confirms the correctness of calculations reported here [3].

Finally, a comparison of the calculated, time-dependent cooling curves with their experimental counterparts should be made. An example of both calculated and measured data for an arbitrarily chosen surface point of the second stellite layer is shown in Fig. 9. The lowest temperature around 730 °C observed after about 0.33 s results from combination of the time frame and the minimal temperature limit recorded by the pyrometer. The results indicate agreement of the calculated data with experimental ones with an acceptable accuracy of ± 2%.

6. CONCLUSIONS

For the process of multilayer cladding by laser remelting of metal powders the temperature field model was proposed and results of numerical solutions were discussed. A multilayer geometry, depth-dependent temperature variations, and also temperature dependent material constants were considered. The model was applied for calculation of the

temperature distribution in multilayers made of bronze B10 and stellite SF6. Data derived from the calculated, time-dependent solutions were compared with results obtained experimentally for the same materials and discussed.

It was shown that the temperature distribution obtained from the calculations matches the molten pool shape and dimensions observed in the experiment. Values below 9% for the dilution coefficient at interfaces between individual layers, derived from the depth dependent chemical composition, correspond with the depth of remelting concluded from the process modelling. Also, the measured cooling curves are consistent with the calculated counterparts. The model allows one not only to calculate the local temperature field with a given spatial resolution but also to study its temporal evolution in dependence on the process parameters.

The model was successfully tested for two materials of different thermo-physical properties. Also the parameters used in our calculations were experimentally examined and found as the best for both materials applied. However, a further verification of the model by doing extended calculations of the temperature field for a wider range of process parameters and also comparison with experiment is wishful. This work is in progress and will be reported soon.

ACKNOWLEDGEMENTS

This work was sponsored by the State Committee for Scientific Research (KBN) in the years 2002-2004 under contract No. 0809/T08/02/22.

REFERENCES

[1] L. Shepeleva, B. Medres, W.D. Kaplan, M. Bamberger, A. Weisheit, Surface and Coatings Technology 125 (2000) 45.

[2] R. Jendrzejewski, A. Conde, J. de Damborenea, G. Śliwiński, Materials and Design 23 (2002) 83.

[3] R. Vilar, Materials Science Forum 301 (1999) 229.

[4] M. Gremaud, J.D. Wagniere, A. Zryd, W. Kurz, Surface Engineering 12 (1996) 251.

[5] R. Jendrzejewski, Thesis, IF-FM PAS, Gdańsk (2000).

[6] M. Picasso, C.F. Marsden, J.D. Wagniere, A. Frenk, M. Rappaz, Metallurgical and Materials Transactions 25B (1994) 281.

[7] B. Ollier, N. Pirch, E.W. Kreutz, H. Schlueter, A. Gasser, K. Wissenbach, Proc. ECLAT 92 (1992) 687.

[8] A.F.A. Hoadley, M. Rappaz, Metallurgical Transactions 23B (1992) 631.

[9] E. Hoffmann, G. Backes, A. Gasser, E.W. Kreutz, R. Stromeyer, K. Wissenbach, Laser und Optoelektronik 28 (1996) 59.

[10] B.B. Budkowska, I. Kreja, International Journal of Offshore and Polar Engineering 7 (1997) 127.

[11] K.J. Bathe, Finite Elements Procedures, Prentice Hall, Englewood Cliffs, NJ, 1996.

[12] R. Jendrzejewski, A. Conde, J. de Damborenea, G. Śliwiński, Proceedings of SPIE 4184 (2001) 603.

Table 1.

Materials used in experiments and values of the density ρ, melting point temperature T_m, thermal conductivity λ, heat capacity C, and latent heat L used in the calculations

material	ρ [kg/m^3]	T_m [°C]	λ [W/m·deg]	C [J/kg·deg]	L [J/kg]
bronze B10	6.0	1020	42-59	545-785	$1.78 \cdot 10^5$
stellite SF6	8.4	1350	14-45	426-801	$3.1 \cdot 10^5$
carbon steel	7.8	1500	30-60.5	434-1169	$2.7 \cdot 10^5$

Table 2.

Properties and composition of the metal powders used for the preparation of sample coatings

material	shape	grain diameter	chemical composition
bronze B10	spherical	< 60 μm	9÷11% Sn, 88-90% Cu, impurities < 1%
stellite SF6	spherical	≈ 60 μm	51.5% Co /bal./, 19% Cr, 13.5% Ni, 7.5% W, max. 3% Fe, 2.3% Si, 1.6% B, max. 1% Mn, 0.7% C

Figure Captions

Fig. 1. Scheme of the laser interaction region and cross-section of the multilayer.

Fig. 2. Temperature field in the 1st laser-cladded layer of bronze B10 on carbon steel after (a) 0.18 s and (b) 0.27 s.

Fig. 3. Temperature field in the (a) 2nd, and (b) 4th bronze B10 layer on carbon steel after 0.27 s.

Fig. 4. Temperature field in the 2nd laser-cladded stellite SF6 layer on carbon steel after (a) 0.22 s and (b) 0.35 s.

Fig. 5. Temperature field in the (a) 1st and (b) 4th stellite SF6 layer on carbon steel after 0.35 s; for production of the 2-4 layers the laser power was reduced to 80% of the value applied for the first layer.

Fig. 6. The stellite SF6 multilayer: fracture (a), cross-section (b), and a diagram of the consecutive traces (c).

Fig. 7. Changes of the main element contents (% wt) of (a) stellite SF6 and (b) bronze B10 coatings vs. distance from the base-clad interface.

Fig. 8. Calculated cooling curves for consecutively melted layers of (a) bronze B10 and (b) stellite SF6; the melting points of bronze (1020°C), stellite (1350°C) and steel-base (1500°C) are marked by vertical lines.

Fig. 9. Comparison of the experimental and computed cooling curves obtained for the second stellite layer.

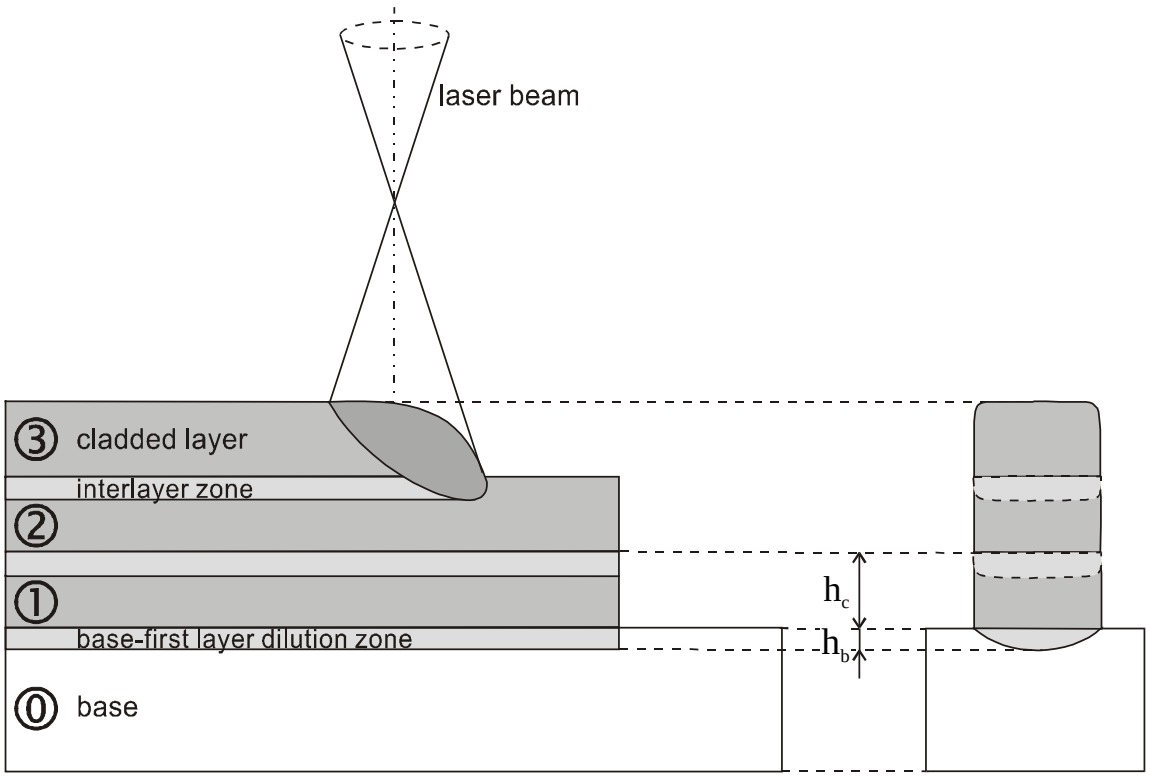

a)

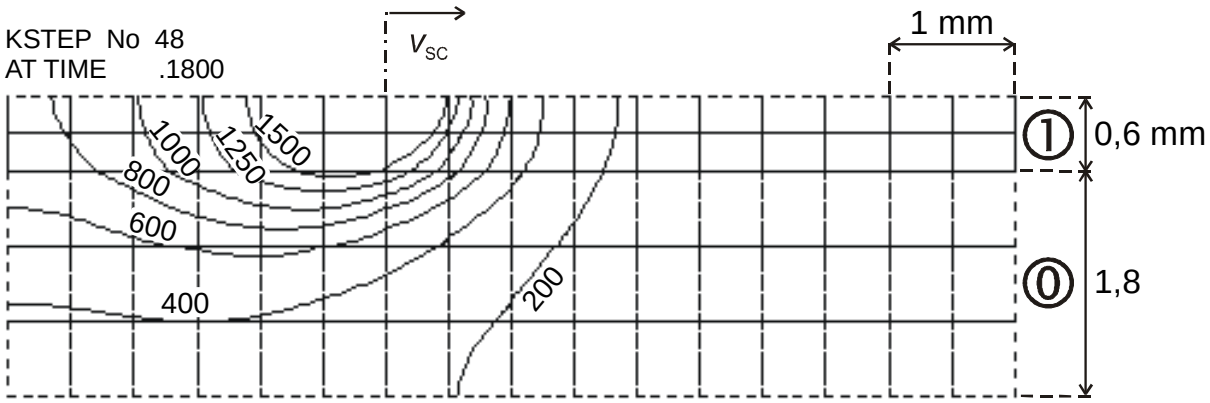

b)

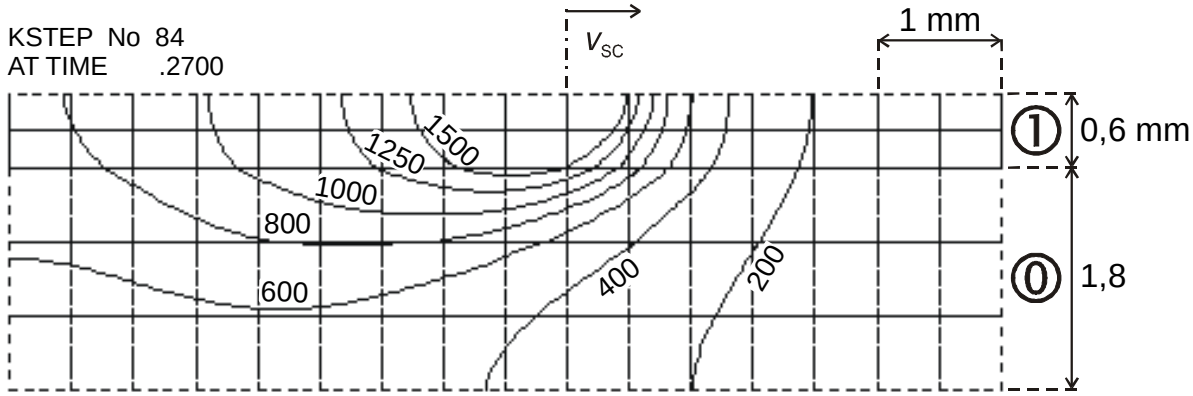

a)

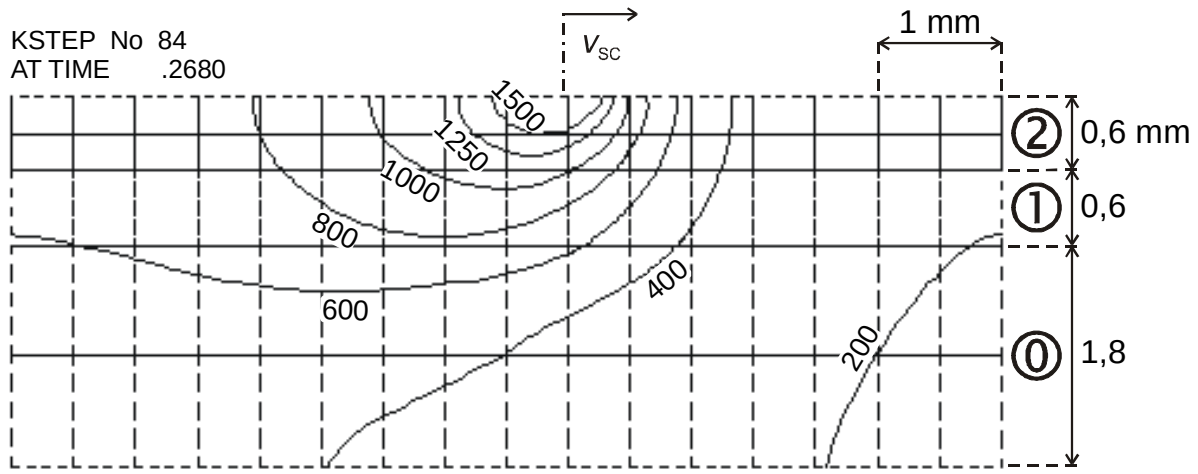

b)

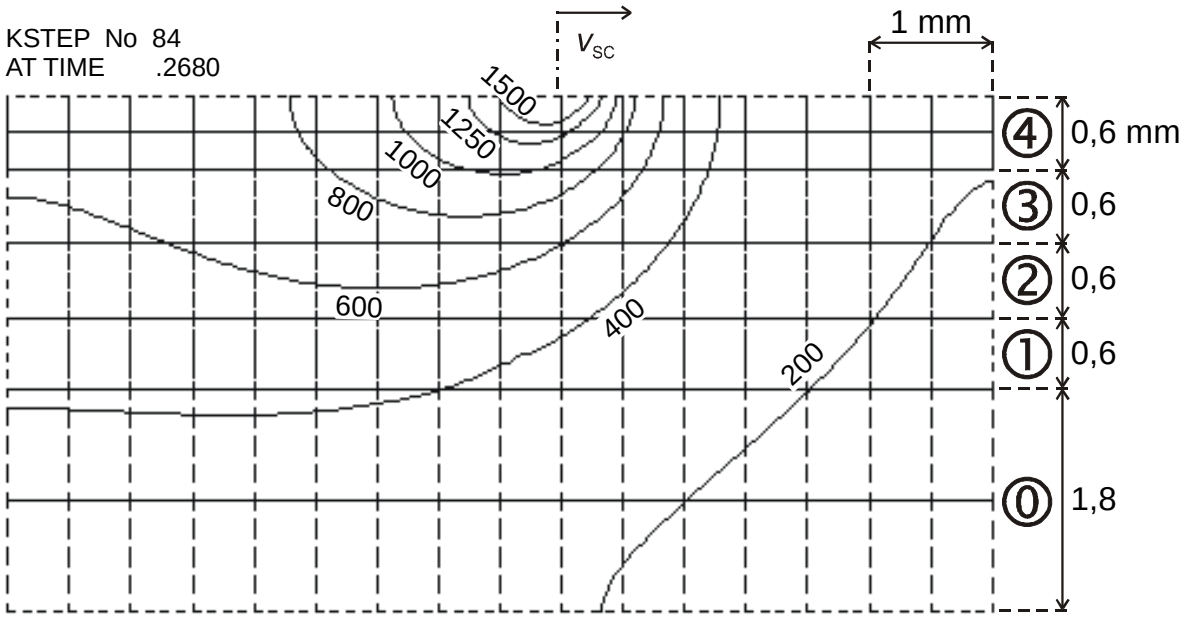

a)

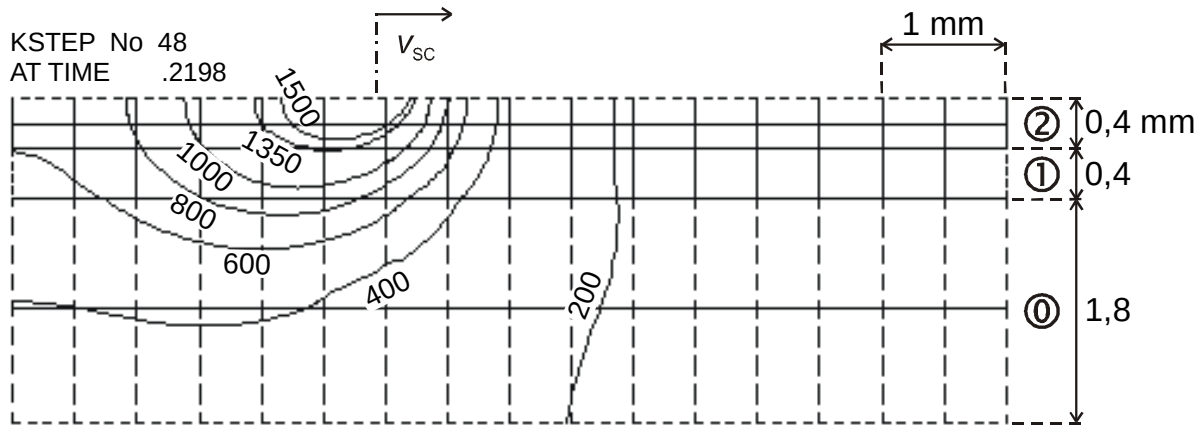

b)

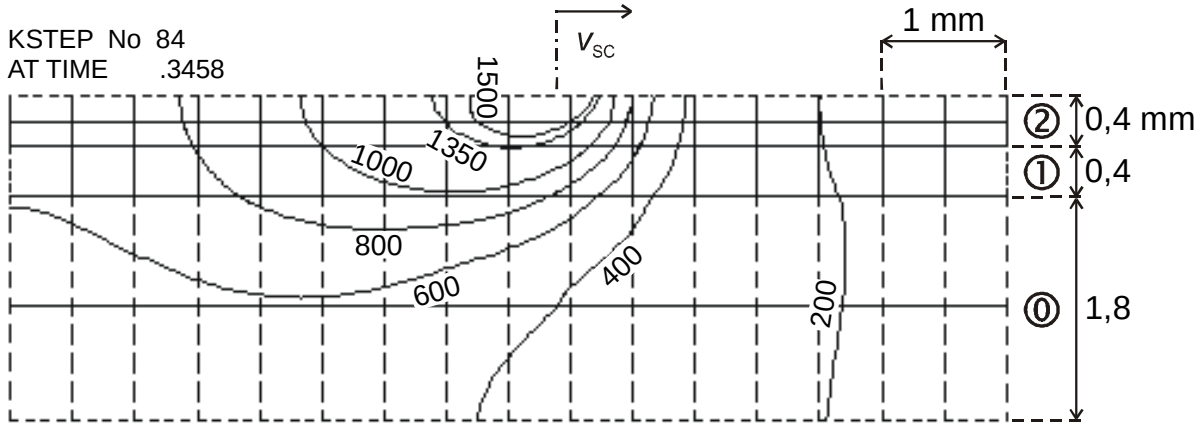

a)

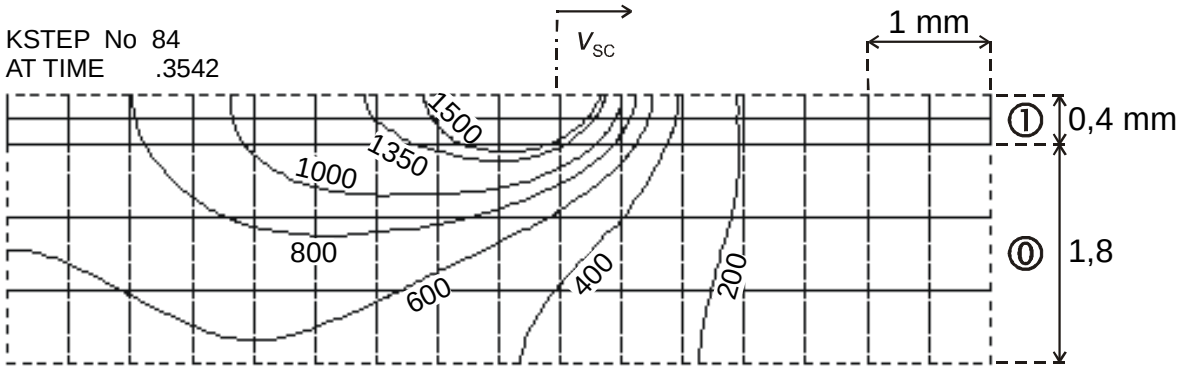

b)

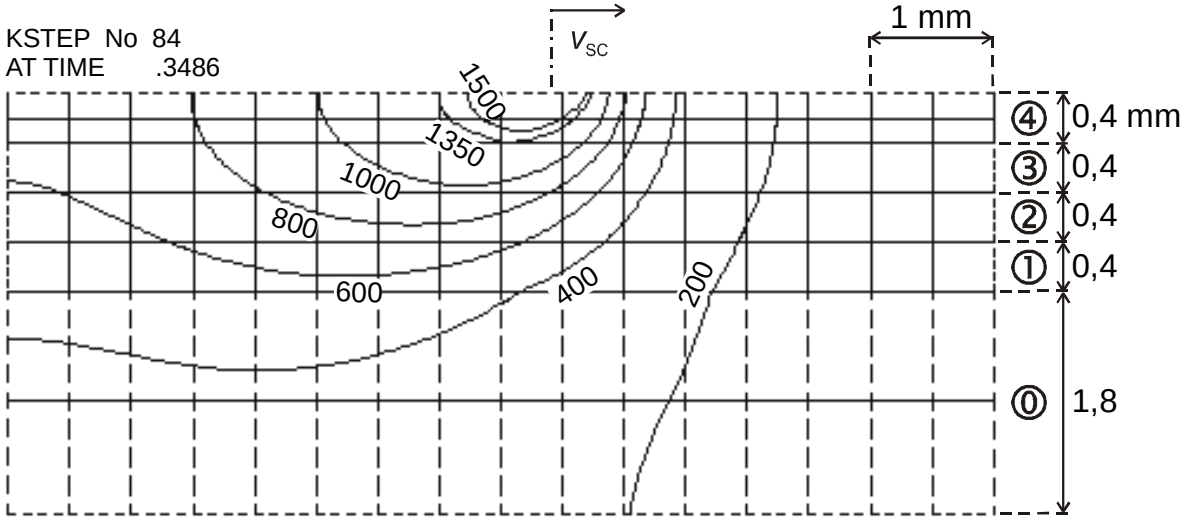

a)

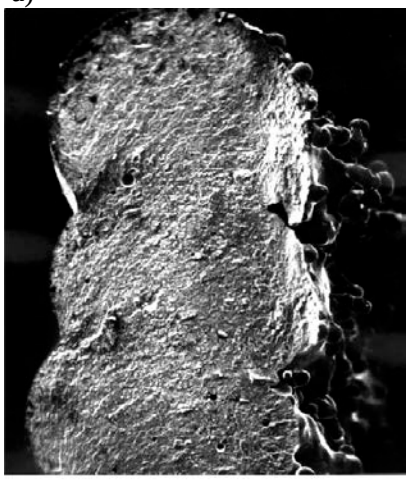

b)

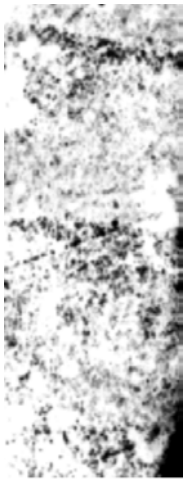

c)

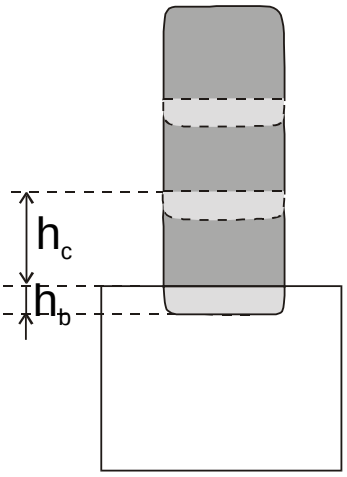

a)

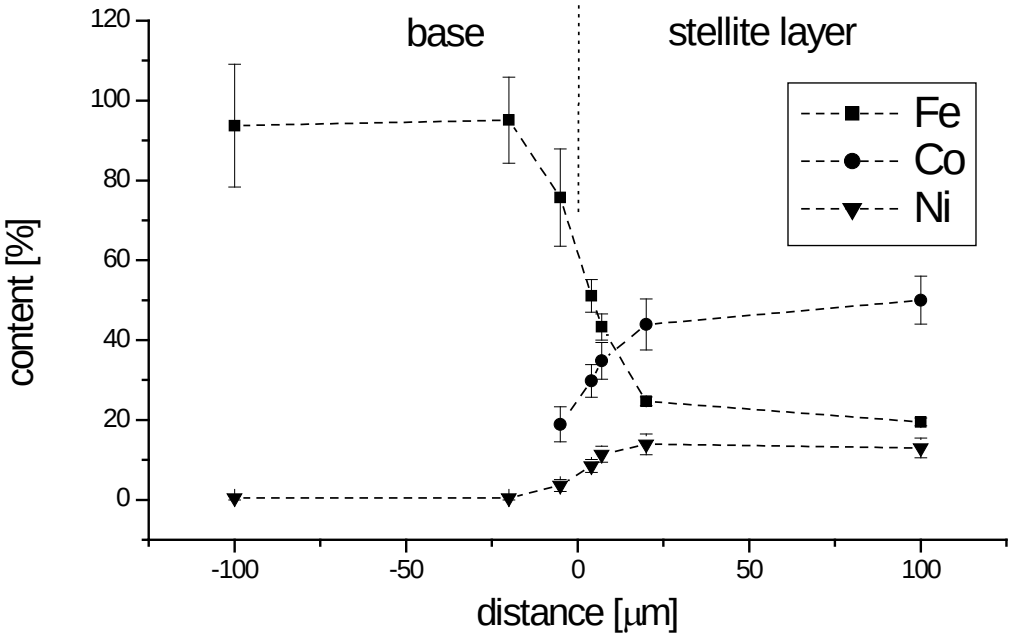

b)

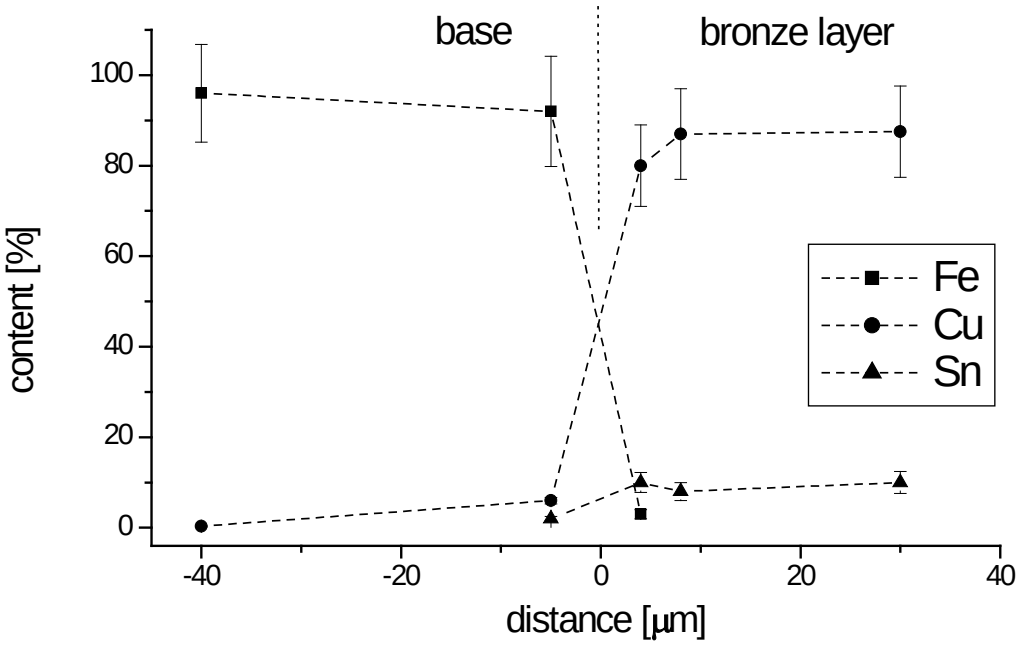

a)

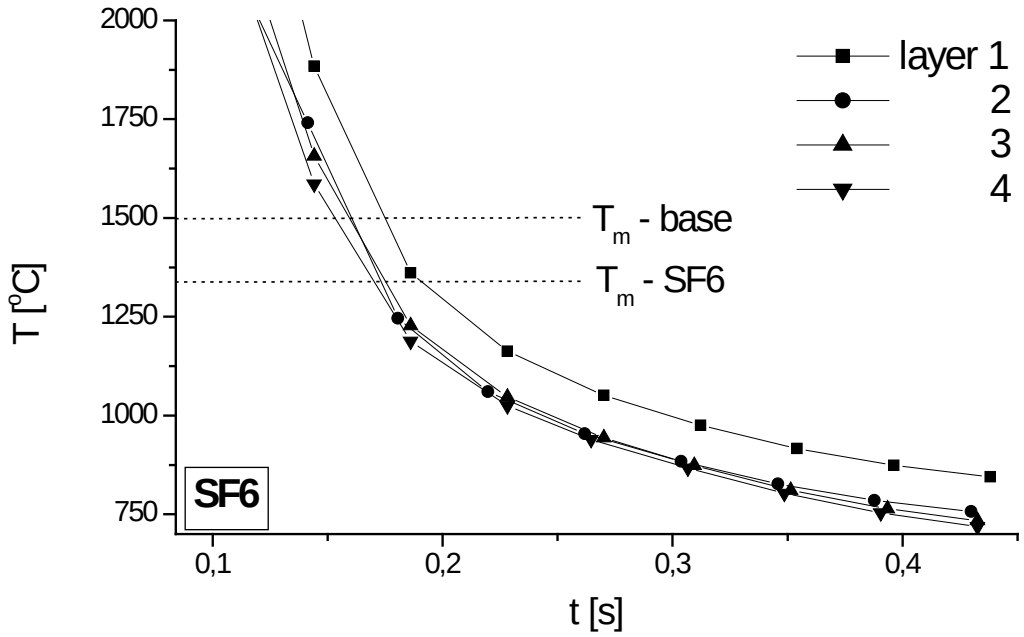

b)